Supplementary Information

Photoreduction properties for Cr (VI) removal of a novel Z-scheme structured $Sr_{0.8}La_{0.2}(Ti^{4+}_{1-\delta}Ti^{3+}_{\delta})O_3/Bi_2MoO_6$ composites

Bin Liu[1,#], Zhili Fan[1,#], Wangjian Zhai[1], Junfeng He[1],Shaofeng Wang[1,*], Fuming Chen[1], Yinzhen Wang[1], Wei Li[1], Xianhua Hou[1], Qinyu He[1,*]

[1]Guangdong Provincial Key Laboratory of Quantum Engineering and Quantum Materials, Guangdong Provincial Engineering Technology Research Center for Quantum Precision Measurement, Guangdong Provincial Engineering Technology Research Center of Efficient Green Energy and Environmental Protection Materials, School of Physics and Telecommunication Engineering, South China Normal University, Guangzhou 510006, China

[#]The authors contributed equally.

[*]Corresponding authors. Email: gracylady@163.com (Qinyu He), wsfxyjs@163.com (Shaofeng Wang)

1. Z-scheme mechanism

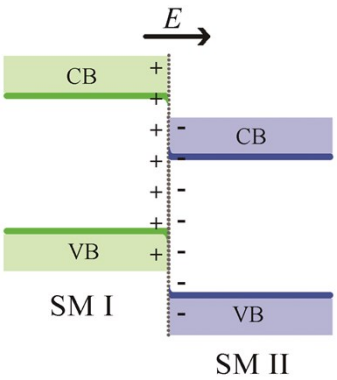

Fig. S1 Illustration of Z-scheme mechanism.

~~1.~~2. Empirical equation of the relation of between the concentration (*C*) of Cr(VI) and the absorbance (A)

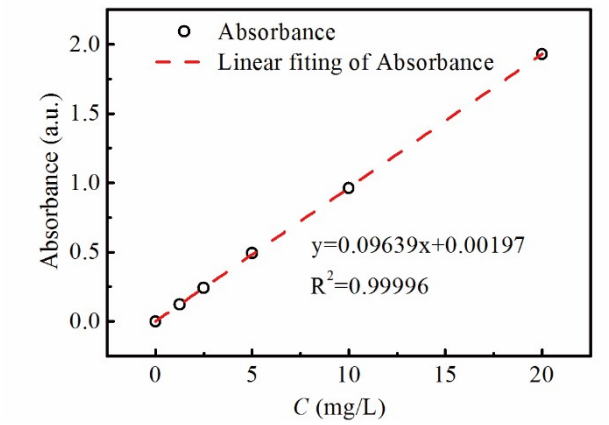

Fig. S2 The relationship between concentration (*C*) and absorbance (A).

3. The Ti^{3+} and O_v amounts with the change in La content.

In order to prove that the Ti^{3+} and O_v amounts increases with the increase of La concentration. As illustrated in **Table S1**, the ratio of the XPS peak area of $Ti^{3+}/(Ti^{4+}+ Ti^{3+})$ and O_v/O_{total} in La-doped $SrTiO_3$ increase with the content of La. The three samples include 10% La doped $SrTiO_3$, 15% La doped $SrTiO_3$ and 20 %La doped $SrTiO_3$. Among them, 20% La doped SrTiO3 is the same sample as LSTO in the manuscript.

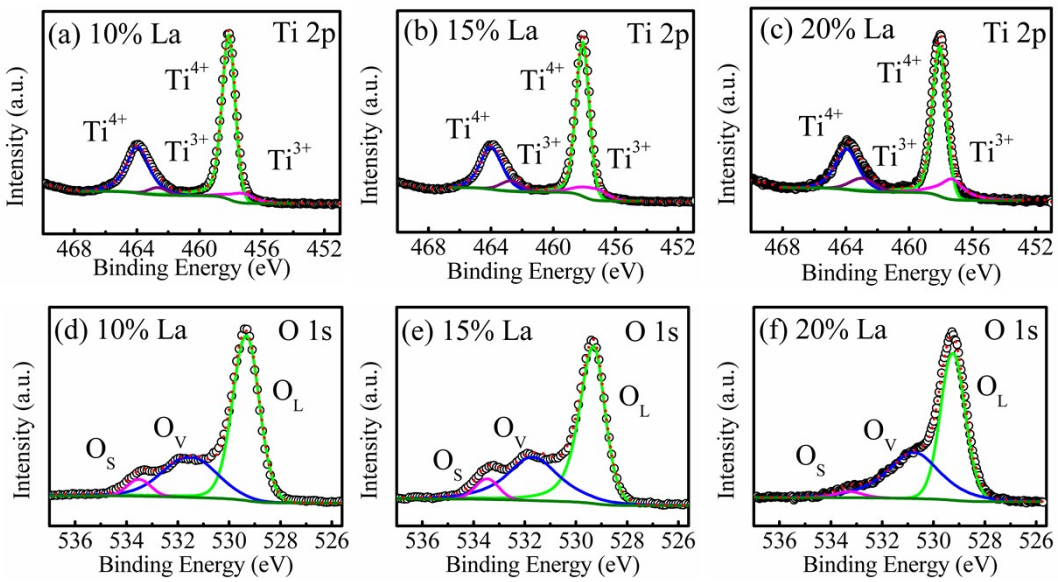

Fig. S3 High-resolution XPS spectra of Ti 2p in (a) 10% La doped $SrTiO_3$, (b) 15% La doped $SrTiO_3$ and (c) 20%La doped $SrTiO_3$; high-resolution XPS spectra of O 1s in (d) 10% La doped $SrTiO_3$, (e) 15% La doped $SrTiO_3$ and (f) 20% La doped $SrTiO_3$ for calculating the amounts of Ti^{3+} and O_v in La-doped $SrTiO_3$ by XPS peak area (O_L-the lattice oxygen of $SrTiO_3$, O_V-the oxygen vacancy of $SrTiO_3$, O_S-the loosely bound oxygen on $SrTiO_3$ surface).

Table S1 The XPS peak areas ratio of the Ti^{3+} and O_v amounts in La-doped $SrTiO_3$ with different La content .

Ratio of La content	**$Ti^{3+}/(Ti^{4+}+Ti^{3+})$(%)**	**O_v/O_{total}(%)**
10%	9.91	29.22
15%	14.53	30.68
20%	20.63	41.01

~~2.~~4. Schematic diagram demonstrating the change mechanism of binding energy of oxygen vacancy in case of build-in electric field

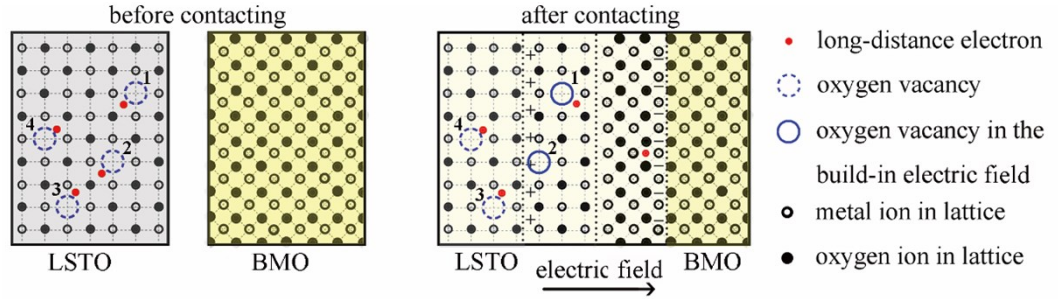

Fig.S2 **Fig. S4**The mechanism of binding energy change of oxygen vacancy in the build-in electric field. After LSTO and BMO contacting, the binding energy of oxygen vacancies located at 530.97 eV and 531.90 eV were marked as 1 and 2, respectively.

It is well known that the oxygen vacancy (O_v) possesses positive charge, the oxygen vacancies would tend to combine long-distance electrons. After the heterojunction LSTO/BMO formed, a built-in electric field would form in the junction, where on the side of LSTO, some O_v closer to the interface would lose the combined electrons and some O_v locating away from the interface wouldn't lose the combined electrons. Consequently, the binding energy of O 1s would possesses reducing value according to this order: the O_v of LSTO in the junction and closer to the interface, the O_v of LSTO in the junction and locating away from the interface, the other O_v of LSTO and BMO outside the junction LSTO/BMO. Thus, in the XPS spectrum of LSTBM7, the peak located at 530.97 eV could be attributed to the oxygen vacancies which didn't lose combined electrons, while the peak located at 531.90 eV could be ascribed to the oxygen vacancies which lost combined electrons. The mechanism is shown in **Fig. S4**.

5. The Band structure analysis

The UV-vis DRS was used to investigate the light absorption and energy band features of SM. the band gap (Eg) of the SM can be calculated from the Equ. :$\alpha h\nu = A(h\nu - E_g)^{n/2}$. The estimated-$E_g$-s of LSTO and BMO are 3.14 eV and 2.84 eV, respectively. In the meantime, Mott-Schottky plots were used to determine the SM type, as well as the band edge positions of LSTO and BMO. The evaluated E_{vb} of LSTO and BMO are 1.75 V and 2.49 V respectively.

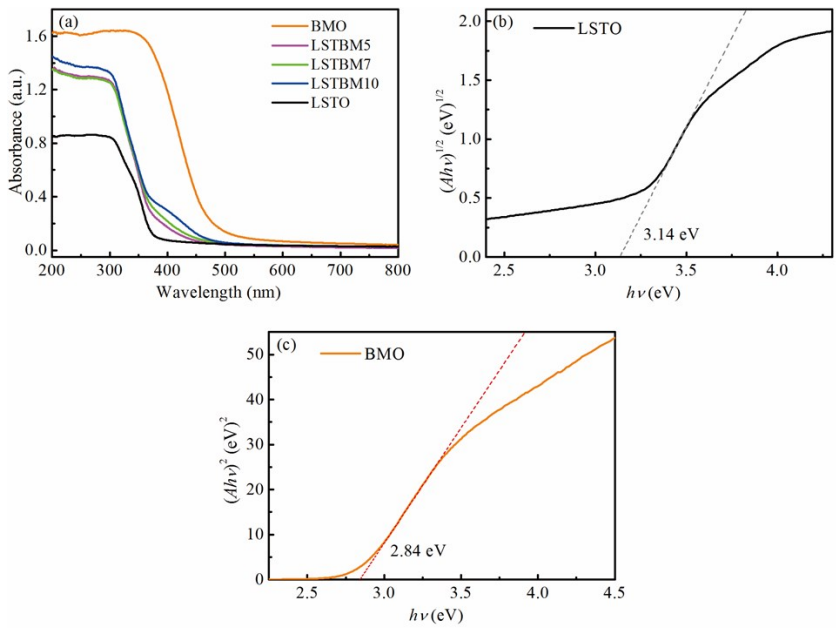

Fig. S5 (a) UV-vis absorbance spectra; (b) Tauc plots of LSTO; (c) Tauc plots of BMO.

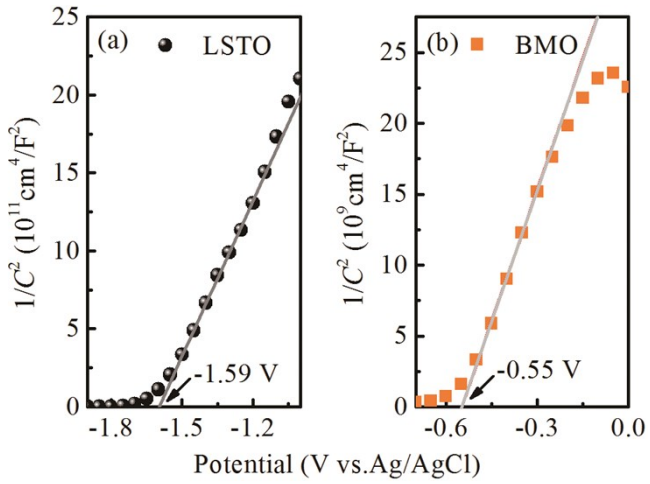

Fig. S6 The Mott-Schottky plots of (a) LSTO and (b) BMO.

6. Possible reaction route to reducing Cr(VI) to Cr(III).

In order to examine reaction route to reducing Cr(VI) to Cr(III), a series of investigation have been performed to compare the compositions and phases between the fresh LSTBM7 and the used LSTBM7.

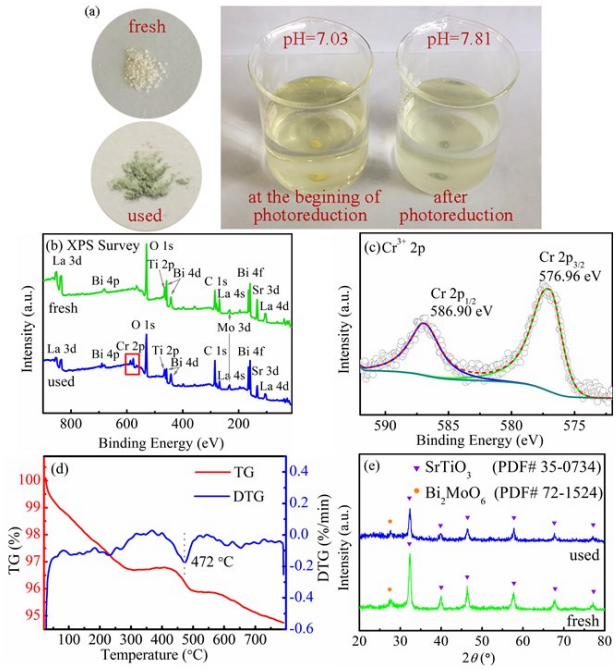

Fig. S7 Comparison of (a) XPS survey spectra, (b) high-resolution XPS spectra of Cr 2p; (c) color of LSTBM7 powder and pH value of two LSTBM7 powders in Cr(VI) solutions before and after photocatalytic Cr(VI) reduction; (d) TG and DTG curves of used LSTBM7; (e) XRD between fresh and used LSTBM7. The word "fresh" and "used" mean the sample, respectively, hasn't and has, been plugged into the simulated waste water-Cr(VI) solution for dark adsorption and photoreduction.

7. Valence state of Cr during photocatalytic reaction

A comparison of high-solution XPS between the samples after 20 min of photoreduction and 180 min of photoreduction.

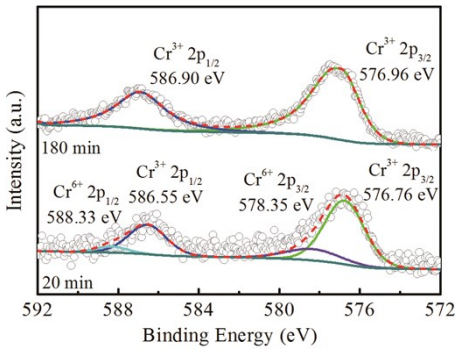

Fig. S8 Composition change of the surface of LSTBM7 particles during photoreduction revealed by the high-resolution XPS.

8. Structural stability of LSTBM7

The structural stability of LSTBM7 was evaluated by ICP-AES during photocatalytic cycle test. As shown in **Table S2**, after three times of photocatalytic reaction, there is few ion leaching from the catalyst.

Table S2 Characterizations of ICP-AES of LSTBM7 during the photocatalytic cycle test.

Cycle	La(mg/L)	Sr(mg/L)	Ti(mg/L)	Bi(mg/L)	Mo(mg/L)
Cycle 1	< 0.00208	0.42418	< 0.00065	< 0.00616	0.38824
Cycle 2	< 0.00208	0.43317	< 0.00065	< 0.00616	0.40717
Cycle 3	< 0.00208	0.44788	< 0.00065	< 0.00616	0.44953